Entanglement Randomness and Gapped Itinerant Carriers in a Frustrated Quantum Magnet

Yuanqi Lyu (吕源祺),[1,*,†] Luke Pritchard Cairns,[1,*] Josue Rodriguez,[1,2] Chunxiao Liu (刘春骁),[1] Kenneth Ng (吴子建),[1] John Singleton,[3] and James G. Analytis[1,2,4,5,‡]

[1]*Department of Physics, University of California, Berkeley, California 94720, USA*
[2]*Materials Science Division, Lawrence Berkeley National Laboratory, Berkeley, California 94720, USA*
[3]*National High Magnetic Field Laboratory, Los Alamos National Laboratory, Los Alamos, New Mexico 87545, USA*
[4]*CIFAR Quantum Materials, Toronto, Ontario M5G 1M1, Canada*
[5]*Kavli Energy NanoScience Institute, Berkeley, California 94720, USA*

(Received 29 April 2025; revised 19 September 2025; accepted 16 October 2025; published 21 November 2025)

The quantum spin liquid is a state manifesting extraordinary many-body entanglement, and the material $NaYbSe_2$ is thought to be one of the most promising candidates for its realization. Through low-temperature heat capacity and thermal conductivity measurements, we identify an apparent contradiction familiar to many quantum spin liquid candidates: While entropy is stored by apparently gapless excitations, the itinerant carriers of entropy are gapped. By studying the compositional series $NaYb_xLu_{1-x}Se_2$ across a percolation transition of the magnetic lattice, we suggest that this contradiction can be resolved by the presence of entanglement scales of random sizes. Moreover, as we truncate the scale of entanglement by magnetic dilution, we show that the itinerant magnetic entropy carrier in $NaYbSe_2$ does not arise from a uniform globally entangled spin ground state but rather materializes through the stochastic propagation of boundaries between locally entangled spin objects.

DOI: 10.1103/tx6t-gbxy

Subject Areas: Condensed Matter Physics, Magnetism, Strongly Correlated Materials

I. INTRODUCTION

Quantum entanglement is a many-body state that cannot be separated into the product of its single particle constituents. One simple example of an entangled spin ground state is a singlet dimer, formed when two $S = 1/2$ spins interact through an antiferromagnetic (AFM) Heisenberg exchange interaction. A quantum spin liquid (QSL) is a ground state of unparalleled many-body entanglement where all spins in a connected lattice are entangled together [1]. Among many interesting theoretical properties, such a system could manifest excitations known as spinons with anyonic statistics beyond the fermions and bosons characterizing the standard model [2]. The realization of this state, however, is usually precluded by the onset of long-range order, which is often favored energetically [3] and, consequently, the ground state in almost every case [1,4]. In this case, the wave function is effectively collapsed into a frozen configuration of spins that spontaneously break the underlying symmetry of the lattice. The many-body entangled state can be brought back into favor—at least in numerical simulations—when strong geometric frustration suppresses conventional ordering, thus allowing a QSL to form within a very specific parameter space of interaction strengths [4–6].

The experimental observation of such an exotic state has proven challenging and controversial. At the root of these controversies is the tendency to insist on characterizing a magnetic system either as long-range ordered (LRO) or as a many-body entangled QSL. We argue that this binary characterization is artificial and that a more accurate description depends on the length scale considered. The scale of entanglement will be limited by material disorder; lattice disorder and randomness not only release the geometric frustration locally, but also induce decoherence and collapse long-range entanglement via an "ordering due to disorder" mechanism [7]. In the past decade, it has been shown both numerically [8,9] and analytically [10] that the interplay between entanglement and the randomness among the exchange interactions would stabilize—instead of a QSL—a valence bond glass (VBG) as the ground state. In lieu of long-range entanglement involving all spins as in a QSL, a VBG consists mostly of tiled spin-singlet dimers,

[*]These authors contributed equally to this work.
[†]Contact author: yuanqilyu@berkeley.edu
[‡]Contact author: analytis@berkeley.edu

as well as the occasional single orphan spins and locally entangled larger-than-dimer clusters scattered among the dimer tilings [9]. This state permits short-range order and entanglement to coexist over different length scales. The question of present interest is how the length scale of entanglement evolves between that of the dimer, the randomness of the VBG, and ultimately one that could host a quantum spin liquid.

Our subject is $NaYbSe_2$, a prime candidate for QSL physics on account of its exemplary properties: Yb^{3+} ions of effective spin-1/2 form 2D equilateral triangular lattices where the $\mathcal{J}_1/\mathcal{J}_2$—the ratio between nearest-neighbor (NN) and next-NN exchange strengths—is calculated to favor a QSL ground state [11–16]. The experimental verification of a QSL in $NaYbSe_2$, however, has yielded conflicting results, similar to the situation for most other QSL candidates [11,17,18]. On the one hand, the key signature of spinons in a gapless U(1) QSL—unusual fermionic thermodynamics in an electrical insulator—appears evident in the heat capacity as a large Sommerfeld coefficient (T-linear behavior) [19], and inelastic neutron scattering (INS) detects a continuum indicative of a spinon Fermi surface [11]. On the other hand, this same excitation is absent in the thermal conductivity, and the INS data simultaneously exhibit peaks corresponding to short-range 120°-AFM order [11]. The coexistence of short-range order and entanglement in INS suggests a mixing of various entanglement length scales, which is in contrast with the clear numerical predictions where a uniform phase—either long-range entanglement or AFM order—prevails as the ground state [6]; real-world spatial disorders and randomness, therefore, must play a significant role in determining the length scales of the entanglement and the corresponding spin ground state.

In this study, we conduct heat capacity and thermal conductivity measurements on the composition series of $NaYb_xLu_{1-x}Se_2$, where nonmagnetic Lu^{3+} ions are uniformly distributed with the Yb^{3+}, connecting through a magnetic percolation transition [20]. While we cannot control the intrinsic randomness in the $NaYbSe_2$, the introduction of Lu^{3+} ions adds tunable artificial disorder and dilutes the once-fully-connected triangular magnetic lattice. This allows us to impose spatial constraints on spin-spin entanglement and tip the intricate balance between randomness and entanglement—separating the excitations originating within regions of long-range entanglement from those produced by short-range interactions.

With this approach, we are able to draw several key conclusions from our data. In heat capacity, a peak at around 2 K is observed in all compounds; the majority of entropy is released through this peak, demonstrating the population dominance of the dimer throughout the composition series. A much broader shoulder feature rises at lower temperatures for near-unitary x—in accordance with the enhanced formation of locally entangled large clusters when magnetic dilution and spatial interruptions are minimal. These two features, along with their population evolutions, suggest that a VBG is the ground state. Meanwhile, a gapped magnetic entropy carrier can be identified in the thermal conductivity: It emerges sharply around the percolation transition of the magnetic lattice and remains dominant at higher x—proving its itinerant nature and magnetic origin. Surprisingly, the population of these carriers peaks around the percolation transition, confirming that it cannot arise from any long-range entangled objects but rather from short-range connectivity. We propose that this carrier arises from the non-spin-carrying low-energy excitations of VBG, which emerge at the boundaries between different spin features. Given that randomness and disorder are ubiquitous, our discovery could help explain similar behaviors and controversies common to many other QSL candidates.

II. RESULTS

A. Heat capacity

Shown in Fig. 1 is the zero-field magnetic heat capacity of the compositional series $NaYb_xLu_{1-x}Se_2$. In the $x = 0.05$ compound, the heat capacity peak is almost entirely attributable to isolated dimers collapsing into their respective singlet ground states. The position of the peak, thus, defines the energy scale of interaction, and the data are fit well by a Heisenberg model with $\mathcal{J}/k_B \approx 6.1$ K. (Included in Supplemental Material [21] are more sophisticated attempts to constrain the spin Hamiltonian through modeling the heat capacity and magnetization of $NaYb_{0.05}Lu_{0.95}Se_2$. Supplemental Material [21] also cites Refs. [19,22–31].)

With increasing x—or density of the magnetic Yb^{3+}—the probability for an isolated spin decreases. The heat capacity correspondingly releases more entropy, following the predicted population of connected spins (Fig. 1 inset) and the expectation that isolated spins do not release entropy without an external field. The agreement between the measured entropy release and predicted population of connected spins further confirms that the mixture of Lu^{3+} and Yb^{3+} in our composition series is spatially uniform. By $x \geq 0.4$, almost all spins are connected to neighboring magnetic sites and the released entropy saturates.

In terms of the shape of the heat capacity curves, all measurements for $x \leq 0.5$ appear qualitatively similar to the dimer peak in $NaYb_{0.05}Lu_{0.95}Se_2$, and all can be fit through a simple dimer model with the energy levels being continuously broadened with increasing Yb^{3+} ion density. However, it is important to note that a collection of small clusters—including entangled objects larger than a dimer, with concentrations according to x (see Supplemental Material [21])—can describe the data equally well. Regardless, at the opposite end of the series ($x = 1$), the data appear qualitatively different, and a broad feature is

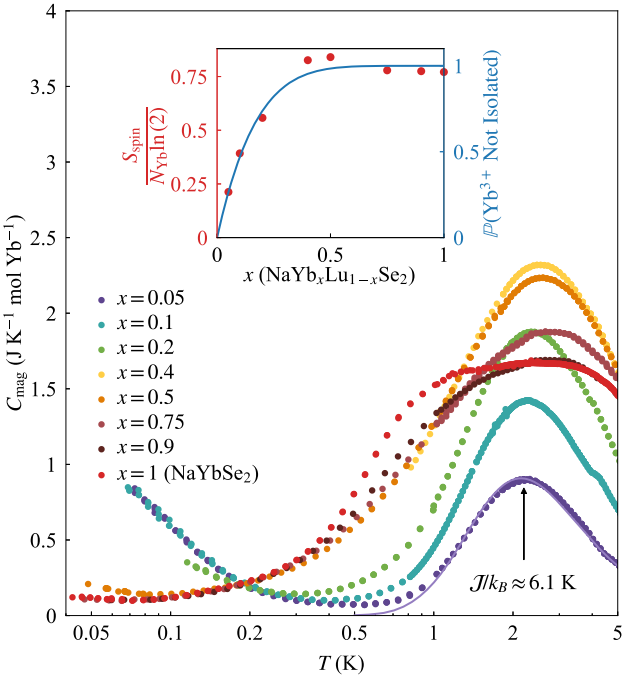

FIG. 1. Magnetic heat capacity of $NaYb_xLu_{1-x}Se_2$ at zero field. The nonmagnetic contribution has been subtracted, assuming it is identical to the $NaLuSe_2$ heat capacity in all cases [20]. The solid line shows a fit to a Heisenberg model with $\mathcal{J}/k_B = 6.1$ K for the $x = 0.05$ compound, as described in the main text and Supplemental Material [21]. Inset: Left axis: the integrated entropy release from electronic spins of the Yb^{3+} between 0.5 and 30 K, plotted as a fraction of the anticipated entropy release according to the number of $J = 1/2$ spins—ln(2) per spin. Right axis: the probability that a Yb^{3+} ion will have at least one Yb^{3+} nearest neighbor and, therefore, is not isolated (see Supplemental Material [21] for details). It is plotted on a different scale compared to the left axis and not a fit of the data.

observed at approximately 1 K, which turns into a shoulder feature with increased dilution ($x = 0.75$–0.9) before becoming unobservable below $x = 0.5$. The position and breadth of this feature suggests that it originates from a magnetic structure with a broad energy spectrum, in contrast to the single energy level ($\mathcal{J}$) associated with the dimer singlet formation. Importantly, the heat capacity contribution from this broad hump is absorbed into the common feature as the system is diluted, as the length scale of connectivity decreases. Given that the length scale of spin correlations is bounded by the continuity of the magnetic lattice—which is rapidly truncated by dilution—this observation suggests the shoulder feature arises from clusters of short-range entangled spins.

B. Thermal conductivity

Shown in Fig. 2(a) is the zero-field longitudinal thermal conductivity for each compound in the compositional series. $NaLuSe_2$ matches the anticipated behavior of a nonmagnetic insulator, with a single $T^{2.3}$ power law below 500 mK. This suppression from the anticipated T^3 phonon behavior is consistent with the thermal conductivity measured in a variety of other nonmagnetic insulators and compounds of similar structure [10,32,33] and is discussed in Supplemental Material [21]. The full magnetic compound $NaYbSe_2$ shows markedly different behavior in the same temperature range, with a thermal conductivity of a significantly smaller magnitude and a bumplike curvature at a low temperature that does not conform to any single power law.

When an external magnetic field of $\mu_0 H = 7$ T is applied parallel to the c axis, as shown in Fig. 3, the thermal conductivity of $NaYbSe_2$ is suppressed and, notably, the bumplike curvature disappears, leaving behind a simple power law that can be attributed entirely to phonons. This implies that the bumplike curvature arises from some additional magnetic contribution that is suppressed by the application of the field. We, thus, model the zero-field thermal conductivity as a combination of a phonon power law κ_{ph} and a gapped magnetic itinerant entropy carrier κ_{mag}, following Ref. [17]:

$$\kappa = \kappa_{ph} + \kappa_{mag} = A_{ph} T^{\alpha} + A_{mag} \exp\left(-\frac{\Delta}{k_B T}\right). \quad (1)$$

We fit this model—with added consideration on spatial dimensionality of the magnetic carrier in the expression for κ_{mag}—to the thermal conductivity of $NaYbSe_2$. See Supplemental Material [21] for details, which includes Refs. [34–36]. The gap is extracted to be $\Delta/k_B \approx 270$mK. The fitted phonon contribution has an exponent α that is similar both to that of $NaYbSe_2$ at $\mu_0 H = 7$ T and $NaLuSe_2$, which further justifies our model. Application of even larger fields, however, would cause the thermal conductivity to rise as the spins become polarized and the phonon scattering is consequently reduced, as has been observed in previous studies on $NaYbSe_2$ [37] and related compounds [38,39].

Applying Eq. (1) to all thermal conductivity results, we obtain the fit parameters, shown in Figs. 2(b)–2(d). A table of all optimal fit parameters and their uncertainties can be found in Supplemental Material [21]. For clarity, we describe separately the main trends observed in each fitting parameter.

(i) A_{ph} [Fig. 2(c)] decreases exponentially with increasing density of magnetic Yb^{3+} sites. This suppression is dramatic—an order-of-magnitude decrease for all temperatures below 1 K, showing very strong phonon scattering that could be linked to lattice disorder [40]. However, the exponential trend is quite peculiar—if it is the mixing of the Yb^{3+} and Lu^{3+} that generates such defects, the end members should be effectively less disordered than the mixed compounds. The systematic decrease with x suggests the

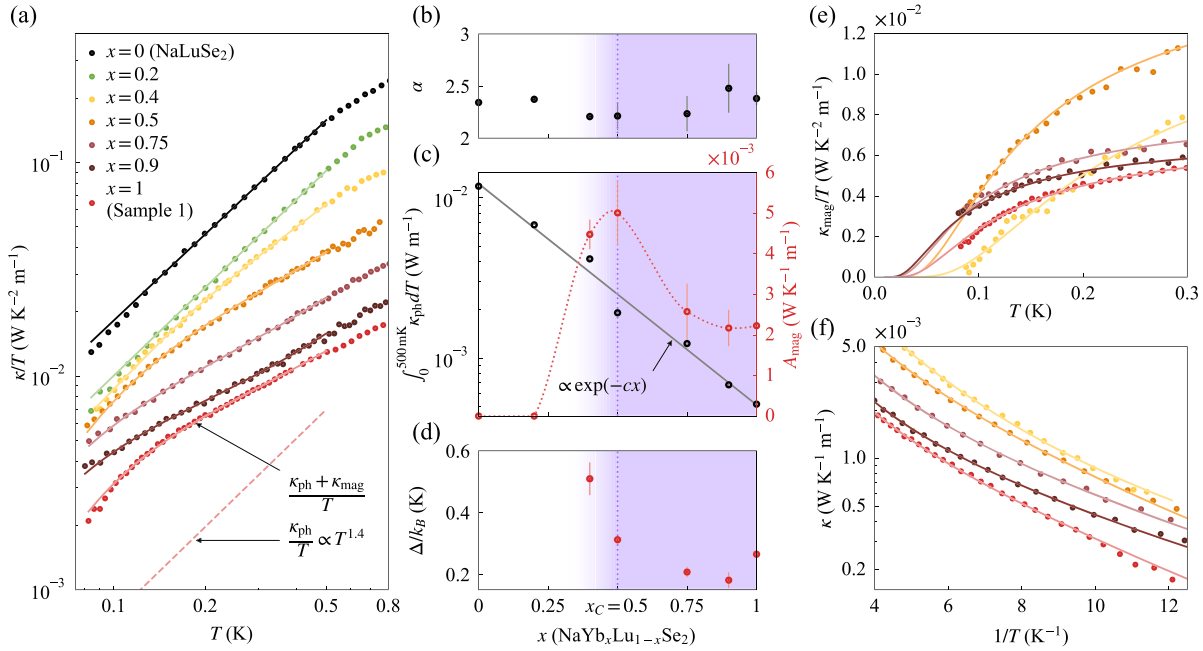

FIG. 2. (a) Zero-field longitudinal thermal conductivity of $NaYb_xLu_{1-x}Se_2$. The solid lines are fits with model described in the main text. The annotated red lines are fits of full thermal conductivity and phonon contributions of $NaYbSe_2$, respectively. (b)–(d) The evolution of fit parameters. The data are fitted using a nonlinear least squares algorithm, and the uncertainties (full lengths of error bars) are obtained as the square roots of optimal fit covariance. To avoid comparing A_{ph} of different units, we plot the integrated κ_{ph} from 0 to 500 mK instead of A_{ph}. The annotated gray solid line is an exponential fit of the integrated κ_{ph} with respect to x; c is a fitting parameter. The red dotted line is a spline to act as a guide to the eye. The percolation threshold is shown as a purple dashed line at $x_C = 0.5$. The purple shaded region ($x \gtrsim x_C$) represents the composition where the magnetic Yb^{3+} lattice is connected. Broadening of the percolation transition is expected in experimental observations due to finite-size effects. (e) Extracted thermal conductivity κ_{mag} of the magnetic entropy carriers. (f) Zero-field thermal conductivity of $NaYb_xLu_{1-x}Se_2$ plotted against $1/T$ on a log scale.

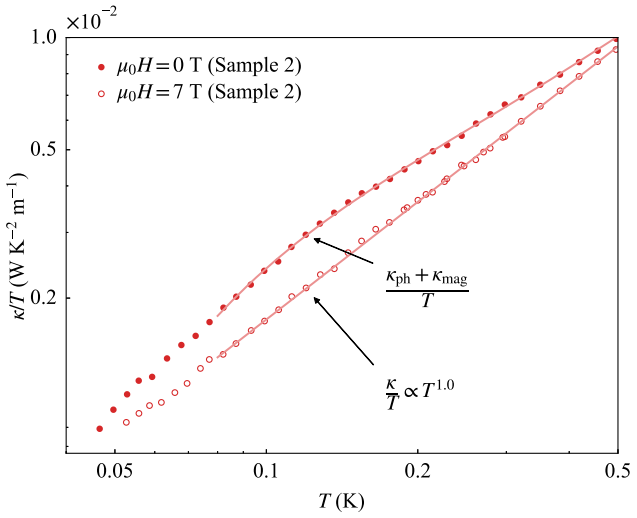

FIG. 3. Thermal conductivity of $NaYbSe_2$ in zero field and in an applied magnetic field of $\mu_0 H = 7$ T parallel to the c axis. The annotated lines are fits to thermal conductivity data, wherein we apply Eq. (1) for the zero-field data and a temperature power law for the in-field data.

strong phonon scattering observed here must be intrinsic to the introduction of Yb^{3+} ions.

(ii) α [Fig. 2(b)] stays relatively constant within fitting uncertainty. This suggests that the phonon scattering evident in A_{ph} is relatively broadband and nonresonant with a specific energy scale (for instance, it cannot be due to interactions with the crystal field energy levels or a single exchange interaction strength). We discuss the possible nature of such phonon scattering in the next section.

(iii) A_{mag} [Fig. 2(c)]—the amplitude of the magnetic contribution—is nonzero only for $x \geq 0.4$, a value that is very close to the percolation threshold of the triangular lattice (which theoretically occurs at $x_C = 0.5$), above which the Yb^{3+} lattice becomes connected. This onset of A_{mag} around the percolation threshold, hence, proves that part of the spin excitation must be itinerant. Perhaps the most striking feature is that A_{mag} appears to peak near the percolation transition where the connected Yb^{3+} lattice is highly disordered: The corresponding magnetic carrier seems to prefer a disordered magnetic lattice over a pristine one.

(iv) Δ [Fig. 2(d)] shows a slight decreasing trend with increasing x. This suggests the origin of the gap is independent of the long-range lattice order but rather linked to some local properties—at the scale of dimer formation.

The extracted thermal conductivity of the magnetic itinerant carriers κ_{mag} is plotted in Fig. 2(e), wherein its exponential nature is evident as a downward curvature. This is obtained by subtracting the smooth temperature power law corresponding to κ_{ph} from the raw measured total thermal conductivity, so as not to introduce any artificial smoothing. Overall, the data show excellent agreement with the model down to the lowest measured temperatures. For smaller values of x, however, the measurement and fitting uncertainties appear larger due to heightened phonon contributions compared to the magnetic contribution. To further illustrate the exponential nature, we plot in Fig. 2(f) the total thermal conductivities κ against inverse temperature $1/T$ on logarithmic scale. Even with the contribution from phonons included, the traces all straighten at low temperatures as the magnetic contributions grow comparatively stronger.

III. DISCUSSION

A. Phonon scattering and quenched randomness

While $NaYbSe_2$ and $NaLuSe_2$ share almost identical structure, lattice constants [20], and molecular weight, as plotted in Fig. 5, the phonon thermal conductivity κ_{ph} in $NaLuSe_2$ is approximately 20 times that of $NaYbSe_2$ below 500 mK. Furthermore, the parameter A_{ph}, which measures the phonon contribution to the thermal conductivity, decreases exponentially with increasing x. Such broadband scattering in temperature is unlikely to be caused by resonant scatterings between phonons and any magnetic transitions—consistent with the comparably small change in total thermal conductivity of $NaYbSe_2$ when an external field is applied (Fig. 3). Rather, the increased phonon scattering must arise intrinsically from the interaction between individual Yb^{3+} ions and the lattice. Strong spin-charge coupling—a key feature of many prominent QSL candidates—has been observed to induce strong quenched randomness [8,41,42]. While the exact microscopic form of spin-charge interaction can vary among materials, its effect on phonon thermal conductivity can be modeled straightforwardly through the Debye-Callaway model [40,43]. From this, a broadband reduction in the mean free path of phonons is expected at low temperatures (see Supplemental Material [21] for details, which includes Refs. [44–48]), and—as plotted in Fig. 5—our simulation of this effect describes the measured data well. This strong phonon scattering is also observed in the related system $YbMgGaO_4$, whose phonon thermal conductivity is about one-fourth that of the nonmagnetic $LuMgGaO_4$ [38]—we include a discussion of their thermal conductivity in Supplemental Material [21], which includes Ref. [49]. The important point for the present argument is that quenched randomness is likely intrinsic to the Yb^{3+} lattice and decreases precipitously as the lattice is diluted of Yb^{3+} ions.

B. Valence bond glass

Quenched lattice disorder translates into randomness in the exchange parameters. A number of previous studies [8–10,50] have shown both numerically and analytically that the same (or very similar) random-bond-strength Hamiltonian will yield a VBG ground state. This is characterized by a distribution of entangled objects of mostly spin singlets tiled around larger-than-dimer entangled clusters and orphan spins. The effect of dilution x will only enhance the randomness of the exchange, stabilizing the VBG ground state [8] and spin-glass physics, in general [7,51,52].

The coexistence of both dimers and clusters is vivid in the heat capacity data of $NaYbSe_2$, which exhibits an initial peak at the same temperature that dimers form, followed by a broad shoulder feature at lower temperatures corresponding to the formation of larger clusters. As the addition of Lu^{3+} ions breaks up the fully connected magnetic lattice, the length scale of spin-spin entanglement becomes physically bounded. Consequently, a sharp decrease in the population of the clusters—which are more space sensitive—is observed as a rapid shrinking of the shoulder feature with decreasing x, leaving just an engorged dimer peak as the system is diluted. We illustrate the change in the ratios between dimers and clusters (akin to the VBG proposal) with different compositions in Fig. 4, with the measured heat capacities plotted alongside.

C. Itinerant magnetic entropy carrier

The existence of an itinerant magnetic entropy carrier is evident in thermal conductivity from a comparison of the in-field and zero-field traces of $NaYbSe_2$, as well as the emergence of the bumplike curvature near the percolation threshold. Intriguingly, the highest population of the itinerant magnetic carrier—the maximum of A_{mag} in Fig. 2(c)—appears near the percolation transition, where the population of locally entangled clusters is comparatively small. The itinerant magnetic entropy carrier is, therefore, unlikely to be a result of the entangled clusters, since these would be maximized at $x = 1$, while the itinerant magnetic carriers are minimized—a direct illustration that the degrees of freedom that store heat differ from those that carry it. On the contrary, the itinerant magnetic carrier seems to prefer a connected but disordered magnetic lattice wherein entangled clusters are minimized and tiled dimers are the dominant magnetic feature.

This is consistent with the VBG picture whereby the majority of magnetic excitations (frozen dimers and

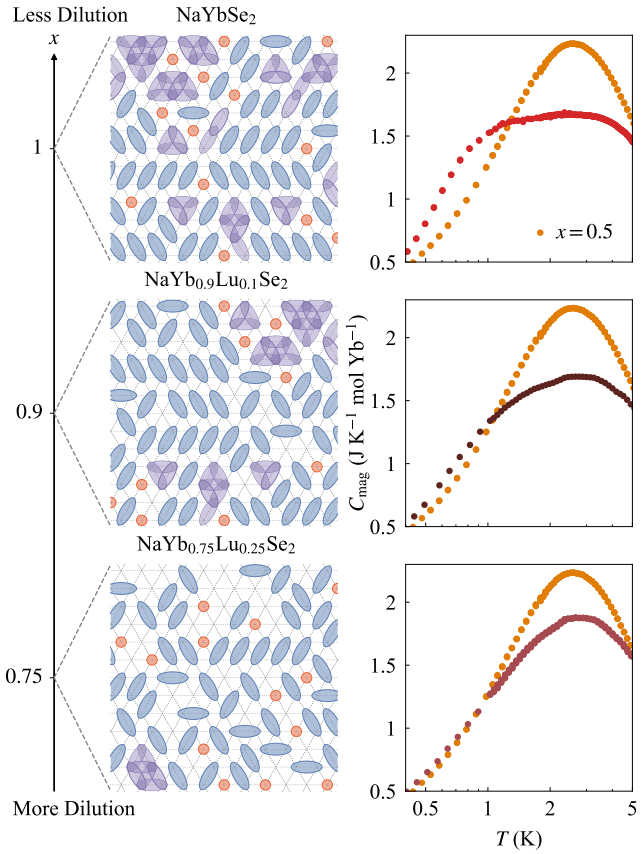

FIG. 4. Left: Illustration of configurations of entangled spins at different compositions and magnetic site dilutions, where the red circles are orphan spins, blue ovals are spin-singlet dimers, and purple regions are locally entangled clusters. The unshaded nodes are Lu^{3+} ions, whose position is assigned randomly according to the expected composition. Right: The corresponding magnetic heat capacities of each composition. The heat capacity of $x = 0.5$ ($NaYb_{0.5}Lu_{0.5}Se_2$) is plotted as the orange points in each for comparison.

clusters) are limited by their physical size and are not itinerant [10]. However, this leaves open the question of the underlying nature of the magnetic carrier. Motivated by exact diagonalization studies of the low-energy excitations of the VBG in Ref. [9], we suggest an intuitive picture of "entanglement retiling," which offers two mechanisms of itinerant magnetic entropy carriers. In the first case, as illustrated in Fig. 5, table row I, a series of correlated dimers flip along an existing domain wall like dominoes; the flipping terminates at orphan spins [9,10]. In the second case, as illustrated in Fig. 5, table row II, a cluster expands by absorbing nearby dimers and orphan spins [9]. Both processes allow entropy to travel without a spin flip by shifting the boundary of correlated or entangled regions in a one-dimensional fashion. This mechanism also explains the preference of this carrier to lattice disorder, since intuitively the disorder should encourage the creation of boundaries in the form of dimer tiling domains and cluster boundaries. A more detailed modeling of the thermal conductivity is included in Supplemental Material [21].

Since these low-energy excitations do not necessarily require a spin flip (singlet to triplet transition), their energy is not tied to the average nearest-neighbor spin-spin exchange interaction strength $\mathcal{J}$ [10]. Instead, the physical distinction between the ground state and the excited state is characterized by the bond configuration of the dimers. The energy difference between the two states is then governed by the average exchange randomness between the neighboring bonds [10]. This is consistent with the trend of increasing gap size Δ in the thermal conductivity as one approaches the percolation transition and dilution deepens the random potential [Fig. 2(c)]. (See Supplemental Material [21] for a more detailed discussion on the mechanism of the itinerant entropy carrier.)

When an external magnetic field is applied, the orphan spins and nonsinglet ($J_{\text{total}} \neq 0$) clusters become polarized. This lifting of degeneracies increases the energy differences among different spin configurations, discourages the mobility of individual magnetic features including boundaries, and, consequently, reduces the population of itinerant low-energy magnetic entropy carriers. In the thermal conductivity, this manifests as a drastic decrease in the gapped itinerant magnetic excitations and instead a clean power law attributable exclusively to phonons (open points in Fig. 3).

The gapped itinerant magnetic excitation—a natural outcome of the diverse entanglement landscape in a VBG ground state—provides a self-consistent explanation for the observed exponential thermal conductivity and unifies its field, composition, and percolation dependencies. It is worth mentioning that spin-phonon decoupling or scattering can lead to a decrease of the thermal conductivity at low temperatures [39,53–57]. However—as demonstrated in Supplemental Material [21]—neither can reproduce the observed exponential behavior. Instead, both generate power-law dependencies that are incompatible with our observations [Figs. 2(e) and 2(f)]. In principle, one can fine-tune either effect—for instance, multiple spin excitations scattering phonons resonantly at different strengths—to mimic the exponential behavior as a sum of multiple power laws, but this approach fails to explain the field or composition dependence of the thermal conductivity and introduces additional unsubstantiated fitting parameters.

D. Implications

The above picture suggests a resolution to the dilemma of how entangled objects that are localized due to disorder may, nevertheless, have an emergent, itinerant carrier arising from the motion of their boundaries in $NaYbSe_2$. We establish this by recognizing an apparent contradiction that arises in many QSL candidates: a large low-temperature heat capacity that suggests a gapless excitation but a thermal conductivity that appears gapped [17,33,38,39,58–63]. In $NaYbSe_2$, both of these aspects

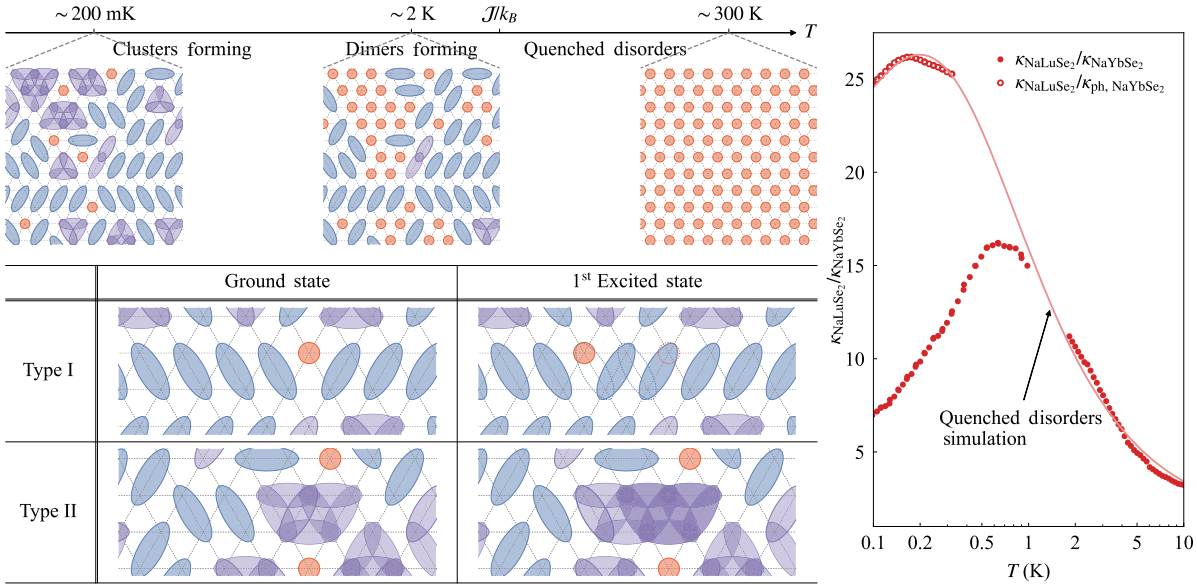

FIG. 5. Top: Illustrations of the spin configurations in $NaYbSe_2$ at different temperatures, following the same color convention as in Fig. 4. Table: Two types of low-energy excitations that can lead to an itinerant magnetic entropy carrier. In the right column, the original spin features are overlaid as dashed lines to visually assist the comparison. Right: The ratio of thermal conductivity between $NaLuSe_2$ and $NaYbSe_2$; the open points are the ratio of thermal conductivity of $NaLuSe_2$ over the fitted phonon thermal conductivity κ_{ph} in $NaYbSe_2$. The solid line is a simulation of the phonon thermal conductivity ratio given extra scattering due to quenched disorders in $NaYbSe_2$.

survive until the onset of a magnetic percolation transition and an itineracy that is, in fact, enhanced by the presence of disorder with a gap that is significantly smaller than the exchange interaction. A recent muon spin relaxation (μSR) study on composition series $NaYb_{1-x}Lu_xO_2$ further substantiates our conclusion, as the authors observed correlated spin excitations for relatively large values of x, leading to the conclusion that the spin ground state is a "quantum disordered state that is robust to magnetic dilution up to the percolation threshold" [64]. Our picture suggests that INS studies on a similar compositional series should yield corroborating results and that one would observe dispersive features even in frustrated quantum magnets with strong site dilutions.

It is important to point out that decades of research into QSLs has yielded many promising material candidates, almost all of which face the same controversy: The entropy carrying and entropy storing degrees of freedom cannot be reconciled—at least not when we insist on a binary characterization of LRO or QSL. However, embracing a picture where the length scale of entanglement is truncated extrinsically is both natural and contains explanatory power. Thermal conductivity measurements as a function of magnetic dilution can play an important role in identifying the mechanism for this truncation and, thereby, help inform future searches for ever-more-promising QSL candidates. In the present case, our expectation is that the spin-charge coupling in $NaYbSe_2$ may be too strong to avoid quenched randomness, and higher material purity could favor either LRO or a QSL. Future searches should, therefore, be directed toward materials where the mechanism for spin-charge coupling is better understood and in which it can be minimized.

ACKNOWLEDGMENTS

We thank Joel E. Moore, Ehud Altman, Itamar Kimchi, Joseph Orenstein, Kamran Behnia, and Vidya Madhavan for helpful discussions. This work was supported by the U.S. Department of Energy (DOE), Office of Science, Basic Energy Sciences, Materials Sciences and Engineering Division under Contract No. DEAC02-05-CH11231 within the Quantum Materials program (KC2202). L. P. C., Y. L., K. N., and J. G. A. were supported by the EPiQS Initiative of the Gordon and Betty Moore Foundation through Grant No. GBMF9067. J. R. was supported by the Quantum Materials program (KC2202) at the Lawrence Berkeley National Laboratory. C. L. acknowledges the fellowship support from the Gordon and Betty Moore Foundation through the Emergent Phenomena in Quantum Systems (EPiQS) program. Work at the National High Magnetic Field Laboratory was supported by NSF Cooperative Agreements No. DMR-1644779 and No. DMR-2128556, the DOE, and the State of Florida. J. S. acknowledges support from the DOE Basic Energy Sciences FWP "Science of 100 T."

DATA AVAILABILITY

The data that support the findings of this article are openly available [65].

[1] C. Broholm, R. J. Cava, S. A. Kivelson, D. G. Nocera, M. R. Norman, and T. Senthil, *Quantum spin liquids*, Science **367**, eaay0668 (2020).

[2] L. Savary and L. Balents, *Quantum spin liquids: A review*, Rep. Prog. Phys. **80**, 016502 (2016).

[3] D. A. Huse and V. Elser, *Simple variational wave functions for two-dimensional Heisenberg spin-1/2 antiferromagnets*, Phys. Rev. Lett. **60**, 2531 (1988).

[4] Z. Zhu and S. R. White, *Spin liquid phase of the* $S = 1/2$ $J_1 - J_2$ *Heisenberg model on the triangular lattice*, Phys. Rev. B **92**, 041105(R) (2015).

[5] J. Iaconis, C.-X. Liu, G. Halasz, and L. Balents, *Spin liquid versus spin orbit coupling on the triangular lattice*, SciPost Phys. **4**, 003 (2018).

[6] Z. Zhu, P. A. Maksimov, S. R. White, and A. L. Chernyshev, *Topography of spin liquids on a triangular lattice*, Phys. Rev. Lett. **120**, 207203 (2018).

[7] Q. Sheng and C. L. Henley, *Ordering due to disorder in a triangular Heisenberg antiferromagnet with exchange anisotropy*, J. Phys. Condens. Matter **4**, 2937 (1992).

[8] K. Watanabe, H. Kawamura, H. Nakano, and T. Sakai, *Quantum spin-liquid behavior in the spin-1/2 random Heisenberg antiferromagnet on the triangular lattice*, J. Phys. Soc. Jpn. **83**, 034714 (2014).

[9] H. Kawamura and K. Uematsu, *Nature of the randomness-induced quantum spin liquids in two dimensions*, J. Phys. Condens. Matter **31**, 504003 (2019).

[10] I. Kimchi, A. Nahum, and T. Senthil, *Valence bonds in random quantum magnets: Theory and application to* $YbMgGaO_4$, Phys. Rev. X **8**, 031028 (2018).

[11] P.-L. Dai *et al.*, *Spinon Fermi surface spin liquid in a triangular lattice antiferromagnet* $NaYbSe_2$, Phys. Rev. X **11**, 021044 (2021).

[12] A. O. Scheie *et al.*, *Proximate spin liquid and fractionalization in the triangular antiferromagnet* $KYbSe_2$, Nat. Phys. **20**, 74 (2024).

[13] A. O. Scheie *et al.*, *Nonlinear magnons and exchange Hamiltonians of the delafossite proximate quantum spin liquid candidates* $KYbSe_2$ *and* $NaYbSe_2$, Phys. Rev. B **109**, 014425 (2024).

[14] Z. Zhang, J. Li, W. Liu, Z. Zhang, J. Ji, F. Jin, R. Chen, J. Wang, X. Wang, J. Ma, and Q. Zhang, *Effective magnetic Hamiltonian at finite temperatures for rare-earth chalcogenides*, Phys. Rev. B **103**, 184419 (2021).

[15] Z. Zangeneh, S. Avdoshenko, J. van den Brink, and L. Hozoi, *Single-site magnetic anisotropy governed by interlayer cation charge imbalance in triangular-lattice* $AYbX_2$, Phys. Rev. B **100**, 174436 (2019).

[16] B. Schmidt, J. Sichelschmidt, K. M. Ranjith, T. Doert, and M. Baenitz, *Yb delafossites: Unique exchange frustration of* $4f$ *spin-1/2 moments on a perfect triangular lattice*, Phys. Rev. B **103**, 214445 (2021).

[17] M. Yamashita, N. Nakata, Y. Kasahara, T. Sasaki, N. Yoneyama, N. Kobayashi, S. Fujimoto, T. Shibauchi, and Y. Matsuda, *Thermal-transport measurements in a quantum spin-liquid state of the frustrated triangular magnet* κ-$(BEDT\text{-}TTF)_2Cu_2(CN)_3$, Nat. Phys. **5**, 44 (2009).

[18] M. M. Bordelon, E. Kenney, C. Liu, T. Hogan, L. Posthuma, M. Kavand, Y. Lyu, M. Sherwin, N. P. Butch, C. Brown, M. J. Graf, L. Balents, and S. D. Wilson, *Field-tunable quantum disordered ground state in the triangular-lattice antiferromagnet* $NaYbO_2$, Nat. Phys. **15**, 1058 (2019).

[19] K. M. Ranjith, S. Luther, T. Reimann, B. Schmidt, P. Schlender, J. Sichelschmidt, H. Yasuoka, A. M. Strydom, Y. Skourski, J. Wosnitza, H. Kühne, T. Doert, and M. Baenitz, *Anisotropic field-induced ordering in the triangular-lattice quantum spin liquid* $NaYbSe_2$, Phys. Rev. B **100**, 224417 (2019).

[20] L. Pritchard Cairns, R. Day, S. Haley, N. Maksimovic, J. Rodriguez, H. Taghinejad, J. Singleton, and J. Analytis, *Tracking the evolution from isolated dimers to many-body entanglement in* $NaLu_xYb_{1-x}Se_2$, Phys. Rev. B **106**, 024404 (2022).

[21] See Supplemental Material at http://link.aps.org/supplemental/10.1103/tx6t-gbxy for experimental methods, as well as detailed modeling and analysis of heat capacity and thermal conductivities of $NaYb_xLu_{1-x}Se_2$ and other quantum spin liquid candidates.

[22] R. Bachmann, F. J. DiSalvo Jr., T. H. Geballe, R. L. Greene, R. E. Howard, C. N. King, H. C. Kirsch, K. N. Lee, R. E. Schwall, H. U. Thomas, and R. B. Zubeck, *Heat capacity measurements on small samples at low temperatures*, Rev. Sci. Instrum. **43**, 205 (1972).

[23] J. S. Hwang, K. J. Lin, and C. Tien, *Measurement of heat capacity by fitting the whole temperature response of a heat-pulse calorimeter*, Rev. Sci. Instrum. **68**, 94 (1997).

[24] G. A. Stewart, *On the interpretation of nuclear quadrupole interaction data for rare-earth nuclei at low symmetry sites*, Hyperfine Interact. **23**, 1 (1985).

[25] R. J. Elliott, K. W. H. Stevens, and M. H. L. Pryce, *The theory of magnetic resonance experiments on salts of the rare earths*, Proc. R. Soc. A **218**, 553 (1953).

[26] A. J. Freeman and R. E. Watson, *Theoretical investigation of some magnetic and spectroscopic properties of rare-earth ions*, Phys. Rev. **127**, 2058 (1962).

[27] R. P. Gupta and S. K. Sen, *Sternheimer shielding-antishielding; Rare-earth ions*, Phys. Rev. A **7**, 850 (1973).

[28] B. Bleaney, *Hyperfine interactions in rare-earth metals*, J. Appl. Phys. **34**, 1024 (1963).

[29] J. R. de Laeter, J. K. Böhlke, P. De Bièvre, H. Hidaka, H. S. Peiser, K. J. R. Rosman, and P. D. P. Taylor, *Atomic weights of the elements. review 2000 (IUPAC technical report)*, Pure Appl. Chem. **75**, 683 (2003).

[30] N. J. Stone, Table of nuclear magnetic dipole and electric quadrupole moments, Technical Report, International Atomic Energy Agency (IAEA). 2014.

[31] V. S. Maryasin and M. E. Zhitomirsky, *Triangular antiferromagnet with nonmagnetic impurities*, Phys. Rev. Lett. **111**, 247201 (2013).

[32] S. Y. Li, J.-B. Bonnemaison, A. Payeur, P. Fournier, C. H. Wang, X. H. Chen, and L. Taillefer, *Low-temperature phonon thermal conductivity of single-crystalline* Nd_2CuO_4*: Effects of sample size and surface roughness*, Phys. Rev. B **77**, 134501 (2008).

[33] Z. Ma *et al.*, *Spin-glass ground state in a triangular-lattice compound* $YbZnGaO_4$, Phys. Rev. Lett. **120**, 087201 (2018).

[34] C. Kittel and P. McEuen, *Introduction to Solid State Physics* (John Wiley & Sons, New York, 2005).

[35] A. V. Sologubenko, K. Giannó, H. R. Ott, U. Ammerahl, and A. Revcolevschi, *Thermal conductivity of the*

hole-doped spin ladder system $Sr_{14-x}Ca_xCu_{24}O_{41}$, Phys. Rev. Lett. **84**, 2714 (2000).

[36] C. Hess, C. Baumann, U. Ammerahl, B. Büchner, F. Heidrich-Meisner, W. Brenig, and A. Revcolevschi, *Magnon heat transport in* $(Sr, Ca, La)_{14}Cu_{24}O_{41}$, Phys. Rev. B **64**, 184305 (2001).

[37] N. Li, M. T. Xie, Q. Huang, Z. W. Zhuo, Z. Zhang, E. S. Choi, Y. Y. Wang, H. Liang, Y. Sun, D. D. Wu, Q. J. Li, H. D. Zhou, G. Chen, X. Zhao, Q. M. Zhang, and X. F. Sun, *Thermodynamics and heat transport in the quantum spin liquid candidates* $NaYbS_2$ *and* $NaYbSe_2$, Phys. Rev. B **110**, 224414 (2024).

[38] Y. Xu, J. Zhang, Y. S. Li, Y. J. Yu, X. C. Hong, Q. M. Zhang, and S. Y. Li, *Absence of magnetic thermal conductivity in the quantum spin-liquid candidate* $YbMgGaO_4$, Phys. Rev. Lett. **117**, 267202 (2016).

[39] X. Hong, M. Gillig, A. R. N. Hanna, S. Chillal, A. T. M. Nazmul Islam, B. Lake, B. Büchner, and C. Hess, *Spinon heat transport in the three-dimensional quantum magnet* $PbCuTe_2O_6$, Phys. Rev. Lett. **131**, 256701 (2023).

[40] P. G. Klemens, *Thermal conductivity and lattice vibrational modes*, in *Solid State Physics* (Academic Press, New York, 1958), Vol. 7, pp. 1–98.

[41] M. Abdel-Jawad, I. Terasaki, T. Sasaki, N. Yoneyama, N. Kobayashi, Y. Uesu, and C. Hotta, *Anomalous dielectric response in the dimer Mott insulator* κ-$(BEDT\text{-}TTF)_2Cu_2(CN)_3$, Phys. Rev. B **82**, 125119 (2010).

[42] M. Abdel-Jawad, N. Tajima, R. Kato, and I. Terasaki, *Disordered conduction in single-crystalline dimer Mott compounds*, Phys. Rev. B **88**, 075139 (2013).

[43] J. Callaway, *Model for lattice thermal conductivity at low temperatures*, Phys. Rev. **113**, 1046 (1959).

[44] R. O. Pohl, X. Liu, and E. Thompson, *Low-temperature thermal conductivity and acoustic attenuation in amorphous solids*, Rev. Mod. Phys. **74**, 991 (2002).

[45] D. G. Cahill, S. K. Watson, and R. O. Pohl, *Lower limit to the thermal conductivity of disordered crystals*, Phys. Rev. B **46**, 6131 (1992).

[46] Z. Zhang, X. Ma, J. Li, G. Wang, D. T. Adroja, T. P. Perring, W. Liu, F. Jin, J. Ji, Y. Wang, Y. Kamiya, X. Wang, J. Ma, and Q. Zhang, *Crystalline electric field excitations in the quantum spin liquid candidate* $NaYbSe_2$, Phys. Rev. B **103**, 035144 (2021).

[47] M. T. Hutchings, *Point-charge calculations of energy levels of magnetic ions in crystalline electric fields*, in *Solid State Physics* (Academic Press, New York, 1964), Vol. 16, pp. 227–273.

[48] M. E. Mullen, B. Lüthi, P. S. Wang, E. Bucher, L. D. Longinotti, J. P. Maita, and H. R. Ott, *Magnetic-ion-lattice interaction: Rare-earth antimonides*, Phys. Rev. B **10**, 186 (1974).

[49] Y. Li, D. Adroja, R. I. Bewley, D. Voneshen, A. A. Tsirlin, P. Gegenwart, and Q. Zhang, *Crystalline electric-field randomness in the triangular lattice spin-liquid* $YbMgGaO_4$, Phys. Rev. Lett. **118**, 107202 (2017).

[50] R. R. P. Singh, *Valence bond glass phase in dilute kagome antiferromagnets*, Phys. Rev. Lett. **104**, 177203 (2010).

[51] L. Liu, H. Shao, Y.-C. Lin, W. Guo, and A. W. Sandvik, *Random-singlet phase in disordered two-dimensional quantum magnets*, Phys. Rev. X **8**, 041040 (2018).

[52] M. Z. Ansari and K. Damle, *Magnetic effects of nonmagnetic impurities in gapped short-range resonating valence bond spin liquids*, Phys. Rev. Lett. **132**, 226504 (2024).

[53] D. J. Sanders and D. Walton, *Effect of magnon-phonon thermal relaxation on heat transport by magnons*, Phys. Rev. B **15**, 1489 (1977).

[54] M. F. Smith, J. Paglione, M. B. Walker, and L. Taillefer, *Origin of anomalous low-temperature downturns in the thermal conductivity of cuprates*, Phys. Rev. B **71**, 014506 (2005).

[55] T. Isono, S. Sugiura, T. Terashima, K. Miyagawa, K. Kanoda, and S. Uji, *Spin-lattice decoupling in a triangular-lattice quantum spin liquid*, Nat. Commun. **9**, 1509 (2018).

[56] S. Bao, Z. Cai, W. Si, W. Wang, X. Wang, Y. Shangguan, Z. Ma, Z.-Y. Dong, R. Kajimoto, K. Ikeuchi, S.-L. Yu, J. Sun, J.-X. Li, and J. Wen, *Evidence for magnon-phonon coupling in the topological magnet* Cu_3TeO_6, Phys. Rev. B **101**, 214419 (2020).

[57] P. Sun, M. Søndergaard, Y. Sun, S. Johnsen, B. B. Iversen, and F. Steglich, *Unchanged thermopower enhancement at the semiconductor-metal transition in correlated* $FeSb_{2-x}Te_x$, Appl. Phys. Lett. **98**, 072105 (2011).

[58] J. M. Ni, Q. Y. Liu, Y. J. Yu, E. J. Cheng, Y. Y. Huang, Z. Y. Liu, X. J. Wang, Y. Sui, and S. Y. Li, *Ultralow-temperature heat transport in the quantum spin liquid candidate* $Ca_{10}Cr_7O_{28}$ *with a bilayer kagome lattice*, Phys. Rev. B **97**, 104413 (2018).

[59] X. Rao *et al.*, *Survival of itinerant excitations and quantum spin state transitions in* $YbMgGaO_4$ *with chemical disorder*, Nat. Commun. **12**, 4949 (2021).

[60] X. Hong, M. Behnami, L. Yuan, B. Li, W. Brenig, B. Büchner, Y. Li, and C. Hess, *Heat transport of the kagome Heisenberg quantum spin liquid candidate* $YCu_3(OH)_{6.5}Br_{2.5}$*: Localized magnetic excitations and a putative spin gap*, Phys. Rev. B **106**, L220406 (2022).

[61] X. Hong, M. Gillig, W. Yao, L. Janssen, V. Kocsis, S. Gass, Y. Li, A. U. B. Wolter, B. Büchner, and C. Hess, *Phonon thermal transport shaped by strong spin-phonon scattering in a Kitaev material* $Na_2Co_2TeO_6$, npj Quantum Mater. **9**, 18 (2024).

[62] C. P. Tu, Z. Ma, H. R. Wang, Y. H. Jiao, D. Z. Dai, and S. Y. Li, *Gapped quantum spin liquid in a triangular-lattice Ising-type antiferromagnet* $PrMgAl_{11}O_{19}$, Phys. Rev. Res. **6**, 043147 (2024).

[63] Z. Zhu, B. Pan, L. Nie, J. Ni, Y. Yang, C. Chen, C. Jiang, Y. Huang, E. Cheng, Y. Yu, J. Miao, A. D. Hillier, X. Chen, T. Wu, Y. Zhou, S. Li, and L. Shu, *Fluctuating magnetic droplets immersed in a sea of quantum spin liquid*, Innovation **4**, 100459 (2023).

[64] S. J. Gomez Alvarado, B. R. Ortiz, S. Bear, B. A. Gonzalez, A. N. Capa Salinas, A. Berlie, M. J. Graf, and S. D. Wilson, *Magnetic dilution in the triangular lattice antiferromagnet* $NaYb_{1-x}Lu_xO_2$, Phys. Rev. B **112**, 144434 (2025).

[65] Y. Lyu, L. Pritchard Cairns, J. Rodriguez, C. Liu, K. Ng, J. Singleton, and J. G. Analytis, *Supporting data for the article entanglement randomness and gapped itinerant carriers in a frustrated quantum magnet* (2025), 10.17605/OSF.IO/CF5UR.